ELSEVIER

^{29}Si MAS NMR Study of the Structure of Calcium Silicate Hydrate

Xiandong Cong and R. James Kirkpatrick
Department of Geology and ACBM Center, University of Illinois at Urbana-Champaign, Urbana

This paper presents the results of a comprehensive investigation of single-phase calcium silicate hydrate (C-S-H) with known compositions using the combined capabilities of ^{29}Si magic angle spinning (MAS) NMR, powder X-ray diffraction (XRD), and chemical analysis of the solution and solid. C-S-H gels with C/S ratios ranging from 0.4 to 1.85 have been synthesized by hydration of highly reactive β-C_2S and aqueous reaction of fumed silica with CaO and separately with highly reactive β-C_2S. The main findings include the following. (1) C-S-H shows continuity and diversity in both composition and structure and forms a continuous structural series. (2) Phase-pure C-S-H has C/S ratios between 0.6–1.54. (3) Si-OH and Ca-OH bonds both occur in C-S-H, with the abundance of the former decreasing and that of the latter increasing with increasing C/S ratio. Model calculation indicates that there are between 0.13–0.43 Si-OH bonds per tetrahedron and the Ca-OH/Ca ratio varies between nearly 0 and 0.64. An ideal formula for C-S-H with a C/S ratio of 1.5 is: $Ca_{4.5}[Si_3O_8(OH)](OH)_4 \cdot nH_2O$. *A defect-tobermorite structural model is proposed for C-S-H in which individual layers have the basic structure of 1.4-nm tobermorite but contain a significant concentration of defects and are more disordered. Stacking disorder between adjacent layer and disorder within individual layers may both contribute to the local and long-range disorder and thus to the diversity of C-S-H.* ADVANCED CEMENT BASED MATERIALS 1996, 3, 144–156

KEY WORDS: C-S-H, Defect-tobermorite structural model, Jennite, NMR, Tobermorite, X-ray diffraction

Calcium silicate hydrate (C-S-H)[1] is an important hydration product of portland cement and controls the strength development of the paste. It has been a major focus of research in cement since for the past four decades but remains poorly understood.

C-S-H can be formed by hydration of C_3S and β-C_2S or alite and belite in portland cement and by precipitation from aqueous solutions containing Ca-salts and silicate. It has a wide range of chemical compositions. Numerous data obtained by bulk chemical analysis [1,2], electron microprobe analysis [3,4], and thermogravimetry [5,6] indicate that its molar C/S ratios vary between 0.6 and more than 2. It is generally accepted that the calcium/silicate (C/S) ratio of C-S-H gel in ordinary portland cement (OPC) paste is in the range of 1.5–2.0 [7], and in most cases near 1.7 [8,9]. The molar H_2O/SiO_2 ratios of C-S-H formed by hydration are between 1.0–1.4 [10], whereas those formed by precipitation are between 0.5–2.5 [11]. Typical water contents of D-dried, fully reacted C_3S are 20–24%, corresponding to the composition $C_{1.7}SH_{1.5}$. C-S-H in nearly saturated OPC pastes contains 42% water, corresponding to the composition $C_{1.7}SH_4$ [8].

Many authors believe that there are different types of C-S-H and have developed structural classifications. An important traditional classification is that of Taylor [1,12], who divided C-S-H into C-S-H(I) and C-S-H(II) and proposed that C-S-H(I) is structurally similar to 1.4-nm tobermorite and C-S-H(II) to jennite [13]. More recently, Jennings [14] observed that the concentrations of lime and silica in aqueous solution in contact with C-S-H fall on two distinct curves in plots of solution CaO concentration against solution SiO_2 concentration. He proposed that the C-S-H phases associated with the two curves are different. ^{29}Si MAS NMR spectroscopy of synthesized C-S-H also appears to show two types of C-S-H [15]. However, these classifications do not generally agree, and the structural classification of C-S-H remains unresolved.

Based on ^{29}Si magic angle spinning (MAS) NMR data, much is now known about the Si-environments in C-S-H and related phases [15–22]. These results have shown that C-S-H in OPC contains only Q^1 and Q^2 Si sites (and possibly some Q^0 sites) but no Q^3 and Q^4 sites. They also indicate that the silicate portion of C-S-H contains only chains and dimers and that no extensive two- or three-dimensional silicate structures are present. Based on this conclusion and X-ray diffraction (XRD) data [23], it is now widely accepted that C-S-H

Address correspondence to: Xiandong Cong, Department of Geology, University of Illinois, 153 Natural History, 1301 West Green Street, Urbana, Illinois 61801.
Received September 1, 1994; Accepted December 12, 1995

[1]Standard shorthand notation in cement science: C, CaO; S, SiO_2; H, H_2O.

ISSN 1065-7355/96/$15.00
PII S1065-7355(96)00023-5

TABLE 1. Chemical composition (mol%), initial and final C/S molar ratio, and XRD phases present for solid samples of the C-S-H series SEWCS and SCFUM

Sample	Initial C/S	SiO_2 (±1%)	CaO (±2%)	H_2O^- (±2%)	H_2O^- (±2%)	Total H_2O	H^+/C	Final C/S	XRD phase
SEWCS1	2.00	16.66	30.78	34.36	18.20	52.56	1.12	1.85	c[a], p[b]
SEWCS2	2.00	16.74	29.59	34.58	19.09	53.67	1.17	1.77	c, p
SEWCS3	2.00	18.53	28.93	32.53	20.03	52.56	1.12	1.56	c
SEWCS4	2.00							1.48[c]	c
SEWCS5	2.00	20.57	28.62	30.12	20.70	50.82	1.05	1.39	c
SEWCS6	2.00							1.27[c]	c
SEWCS7	2.00	25.19	26.77	25.04	23.00	48.04	0.94	1.06	c
SEWCS8	2.00	26.92	26.23	24.02	22.83	46.85	0.92	0.97	c
SCFUMa	2.00	18.94	32.22	27.69	21.15	48.84	0.86	1.70	c, p
SCFUMb	1.80	20.28	31.18	28.95	19.59	48.54	0.93	1.54	c, p
SCFUMc	1.70	21.62	31.24	26.02	21.14	47.16	0.83	1.45	c
SCFUMd	1.50	23.18	30.59	23.59	22.64	46.23	0.77	1.32	c
SCFUMe	1.30	24.20	28.71	22.79	24.31	47.10	0.79	1.19	c
SCFUMf	1.20	21.95	24.82	19.20	34.03	53.23	0.77	1.13	c
SCFUMg	0.90	28.62	25.09	20.23	26.06	46.29	0.81	0.88	c
SCFUMh	0.80	29.35	23.25	20.24	27.16	47.40	0.87	0.79	c
SCFUMi	0.40	41.01	16.72	19.04	23.24	42.28	1.14	0.41	c, s[d]

H_2O^+ is the mole percent weight loss at 1000°C calculated based on a molecular weight of 17 (OH). H_2O^- is the mole percent of weight loss at 110°C calculated based on a molecular weight of 18 (H_2O). H^+/C is the molar ratio of H_2O^+ to CaO. Also given are relative errors in analysis of different chemicals. XRD = X-ray diffraction. [a]c; C-S-H; [b]p; portlandite; [c]estimated based on solution pH; [d]s; amorphous silica.

has a layer structure [24], and structural models based on this idea have been proposed [13,25].

Despite these extensive efforts, the nanostructure of C-S-H is still not fully understood. Important remaining questions include the following. How closely is the C-S-H structure related to those of tobermorite and jennite? How long are the silicate chains, and how homogeneously in length are they distributed? How should C-S-H be classified, and does it form a continuous series or are there different phases?

This paper presents part of the results of a systematic structural study of single phase C-S-H prepared by hydration and pozzolanic reactions [26–29]. The compositions of both the solutions and final solid gels are known. The methods of investigation used include ^{29}Si MAS NMR spectroscopy, powder XRD, and bulk chemical analysis. A defect-tobermorite structural model for C-S-H is proposed in which the Ca-silicate layers resemble those of 1.4-nm tobermorite but contain significant defects and are more disordered.

Experimental

Synthesis of C-S-H

The C-S-H samples have been synthesized through three different routes. All operations were inside a glove bag filled with flowing N_2 gas to prevent carbonation. Water used was deionized and freshly degased by bubbling with N_2 gas to eliminate dissolved CO_2. Solid samples were separated from the solution using 100 circles ashless filter and dried under flowing N_2 gas at room temperature.

The samples of the SEWCS series were made by progressive hydration of highly reactive β-C_2S [30]. Initially, 10 g of β-C_2S were mixed with 500 cc water in a plastic container with magnetic stirring at room temperature. Upon completion of hydration at 40 days, 100 cc of solution and about 1.5 g of solid gel were removed from the container and stored in a separate bottle as sample #1 of the series. 100 cc water was then added. After 2–4 days, 100 cc of the solution was exchanged with 100 cc water. The procedure was repeated until the pH value was about 0.1 less than that of the first sample, when sample #2 was taken.

The samples of the SCFUM series were prepared by aqueous reaction of CaO and fumed silica at initial C/S ratios between 0.4 and 2.0. The CaO was freshly calcined from reagent grade $CaCO_3$ at 1100°C for 2 hours. The fumed silica (99.8% SiO_2; Aldrich Chemical Company, Milwaukee, WI) was also calcined at 1050°C for 15 minutes to remove adsorbed volatiles. Each synthesis run consisted of 200 cc water and 2 g of solid mixture. Plastic bottles containing the samples were sealed and then shaken using a water bath at room temperature for 2 months. The temperature was then raised to 40°C for an additional 4 months.

The samples of the CSHFS series were prepared by reaction of fumed silica with highly reactive β-C_2S. One gram of mixture of fumed silica and β-C_2S with C/S ratios between 0.6 and 1.7 was reacted with 5 cc water

Advn Cem Bas Mat
1996;3:144–156

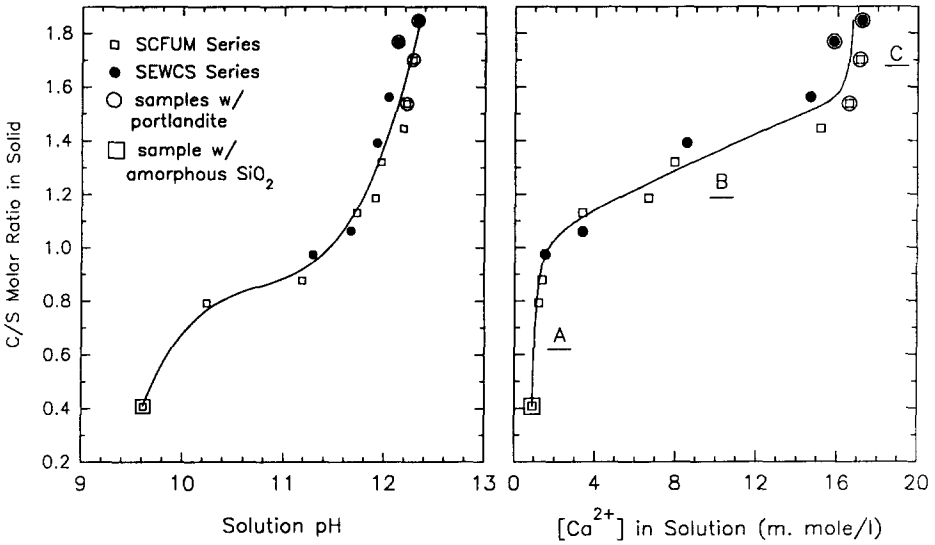

FIGURE 1. Observed relationships between solution pH and C/S ratio of the solid C-S-H (left) and solution Ca^{2+} concentration and C/S ratio of the solid C-S-H (right) for the SEWCs and SCFUM series. Error in pH measurement is 0.01 and Ca^{2+} concentration is about 3%.

in plastic bottles. The sealed bottles were rotated (10 rpm) at room temperature. After 10 months of reaction, the samples became viscous pastes and were dried under flowing N_2 gas at room temperature without filtering.

^{29}Si NMR Experiments

All ^{29}Si NMR spectra were recorded with MAS at room temperature using a home built pulse-Fourier-transform NMR spectrometer equipped with an 8.45 Tesla (Larmor frequency = 71.45 MHz for ^{29}Si) superconducting solenoid magnet and a Nicolet 1280 data system. The probe uses a 7-mm sapphire rotor and was made by Doty Scientific (Columbia, SC).

The MAS frequencies were about 4 kHz, and 200–500 scans were accumulated for each sample, $\pi/3$ pulses and 120 second delays were used. Chemical shifts are reported relative to external TMS, and more negative values correspond to increasing shielding.

Other Experiments

XRD powder patterns were recorded with Cu K_α radiation on a Siemens D-500 diffractometer. A 0.02 2θ step size and 4-second count time were used.

Bulk chemical compositions (CaO and SiO_2) of the solid samples were determined by X-ray fluorescence (XRF) at the Illinois State Geological Survey. Solution chemical compositions were analyzed with inductively coupled plasma (ICP) at the University of Illinois School of Chemical Sciences Microanalytical Laboratory. Solution pH values were measured with a PHB-62 pH meter.

Results

C-S-H Composition

The measured C/S ratios of the solid samples of the SCFUM and SEWCS series range from 0.41 to 1.85 (Table 1), but the largest C/S ratio for single-phase C-S-H (without portlandite) is 1.56. For the SEWCS series, the C/S ratios of the solid decrease with an increasing number of solution changes. For the SCFUM series, the C/S ratios of the solid increase with increasing C/S ratio of the starting materials, but there is a significant difference between the initial and final C/S ratio.

The chemical compositions of the C-S-H samples synthesized by reaction of fumed silica and highly reactive β-C_2S (CSHFS1–CSHFS6) were not analyzed due to small sample size. The C/S ratios cited for these

TABLE 2. C/S molar ratio and XRD phases present for C-S-H samples in the CSHFS series

Sample	CSHFS0[a]	CSHFS1	CSHFS2	CSHFS3	CSHFS4	CSHFS5	CSHFS6
Initial C/S	1.85[b]	1.70	1.50	1.20	1.00	0.80	0.60
XRD	c[c], p[d]	c, p	c	c	c	c	c

XRD = X-ray diffraction.
[a]Fully hydrated highly reactive β-C_2S with w/s = 9 for 11 months; [b]Final C/S inferred from SEWCS1; [c]c; C-S-H; [d]p; portlandite.

samples (Table 2) are the initial values, which should represent their actual C/S ratios, because the hydration products were dried directly without filtering.

For both the SCFUM and SEWCS series, the C/S ratios of the solid samples increase with increasing pH and Ca^{2+} concentration in solution, and the two sample series fall on the same curves (Figure 1). Single-phase C-S-H samples occur between pH = 10 to 12 and Ca^{2+} = 3 to 15.5 mmol/L. The variation of solid C/S ratio and solution pH appears to be continuous, at least for pHs from 10.0 to 12.2. It appears that the samples have reached a metastable (at least) equilibrium state, because the two series react from opposite directions but have the same pH–C/S correlation. The SCFUM samples are formed by net depolymerization of a framework silicate, whereas the SEWCS samples are formed by net polymerization of isolated tetrahedra. Similar results have been reported by Grutzeck et al. [15], who, however, identified two invariant points corresponding to the coexistence of three phases.

Relationships between C/S ratio and solution Ca^{2+} concentration similar to ours have been reported by Taylor [1] and many others [31]. Taylor [1] used a relationship similar to Figure 1 as one of the criteria to distinguish between C-S-H(I) (region B) and C-S-H(II) (region C). Our data indicate that samples with large C/S ratios (region C) are mixtures of C-S-H and portlandite.

The SCFUM and SEWCS samples contain between 42–53 mol% total water, and the total water concentration decreases slightly with decreasing C/S ratio (Table 1). H_2O^+ generally increases with increasing C/S ratio for both analyzed series (Figure 2), indicating a close relationship to at least one portion of the C-S-H structure containing Ca^{2+}. However, the correlations between H_2O^+ and C/S ratio are different for the two series. Samples of the SEWCS series contain more H_2O^+ than those of the SCFUM series, and their H_2O^+ concentrations continuously increase with increasing C/S ratio. The H_2O^+ contents of the SCFUM series samples are independent of C/S ratio for C/S < ca. 1.2 and increase with C/S ratio for C/S >1.2. H_2O^- decreases with increasing C/S ratio for both series. It also decreases with decreasing interlayer spacing as determined by XRD.

XRD Results

Powder XRD shows that most of the samples are phase-pure C-S-H, but portlandite is present for samples with C/S ratios as low as 1.54 (Table 1). The largest C/S ratio of a pure C-S-H phase is 1.56 (SEWCS3). Amorphous silica is present in the sample with the lowest C/S ratio (0.41).

Powder XRD also shows that most of our samples are semicrystalline with some long-range order. Most samples yield at least 5 XRD peaks and some yield up to 13 (Figure 3) . The number of resolvable XRD peaks generally decreases with increasing C/S ratio, indicating decreased long-range structural order. The XRD patterns are dominated by the main C-S-H peaks at ca. 0.307, 0.282, and 0.183 nm, which are present for all samples. Most samples also yield a basal reflection between 0.978 and 1.465 nm, but samples with both large and small C/S ratios sometimes do not.

The observed XRD patterns of the C-S-H are consistent with a layer structure. The average orthorhombic pseudo-cell dimensions of our samples (Table 3) are quite similar to those of 1.4-nm tobermorite [32]. The only difference is the **c** dimension, which increases with increasing H_2O^-. The cell dimensions of 1.1-nm tobermorite and jennite are significantly different than those of our C-S-H samples.

Cell dimensions of C-S-H also change as a function of C/S ratio [33]. The **a** dimension increases and the **b** and **c** dimensions decrease with increasing C/S ratio.

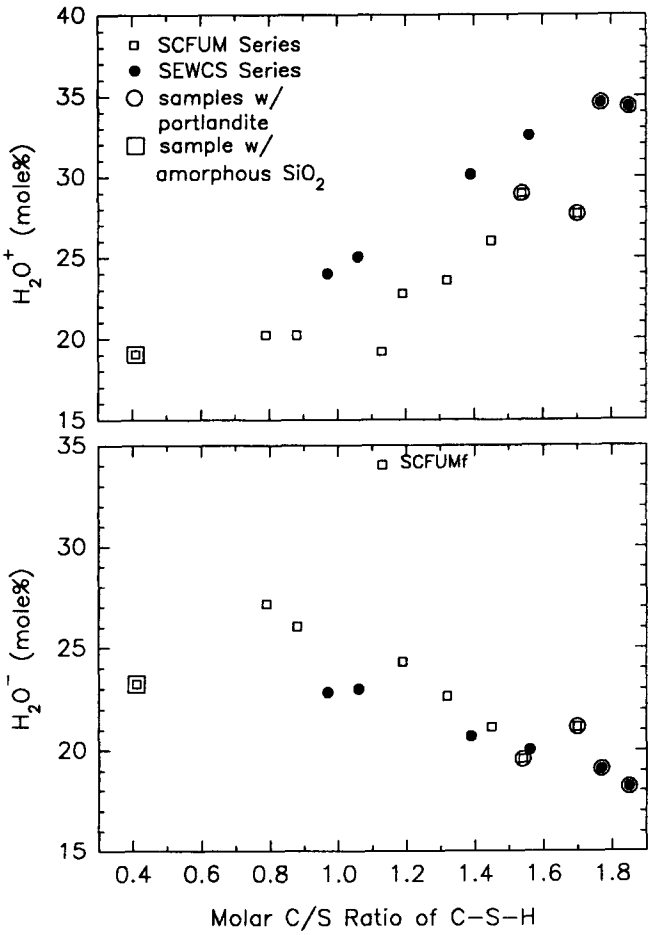

FIGURE 2. Observed relationship between C/S ratio and H_2O^- and H_2O^+ for C-S-H samples of the SEWCS and SCFUM series. The H_2O^- value for sample SCFUMf is likely to be in error.

Advn Cem Bas Mat
1996;3:144–156

TABLE 3. Pseudo-cell data for C-S-H, 1.1- and 1.4-nm tobermorite, and jennite

Phase	C-S-H Range	C-S-H Average	Tobermorite 1.4-nm	Tobermorite 1.1-nm	Jennite
C/S	0.6–1.5		0.90	0.83	1.50
a	0.561–0.566	0.564	0.564	0.559	0.995
b	0.364–0.368	0.366	0.366	0.370	0.364
c	1.975–2.930	2.452	2.806	2.278	2.137
Cell	orthorhombic		orthorhombic	orthorhombic	monoclinic β = 101.91°
Source	this study		ref 32	ref 41	ref 56

Cell dimensions are in nanometers, and C/S is the molar ratio.

^{29}Si MAS NMR Spectroscopy

The ^{29}Si MAS NMR spectra of most of our C-S-H samples contain only two major peaks located at ca. −79.5 and −85.3 ppm (Figure 4), corresponding to Q^1 and Q^2 Si sites respectively [34]. Q^1 sites can be present in pairs of linked silicate tetrahedra (dimers) or at the ends of silicate chains. Q^2 sites are present in the middle of silicate chains. Therefore the main silicate structures in C-S-H, as previously proposed by many authors [16–19,21], are dimers and short silicate chains. There is no evidence in our spectra for the presence of a detectable amount of Q^0 sites (monomers) [21], which would resonate near −71 ppm. The samples with C/S ratios of 0.6 and 0.41 (CSHFS6 and CSFUMi respectively), and probably the sample with C/S = 0.79 (SCFUMh), yield peaks at −94 ppm, corresponding to Q^3 sites. SCFUMi also yields a Q^4 peak located at about −110 ppm, which is readily assigned to Q^4 sites in residual amorphous silica, consistent with the XRD results. The chemical shift of the peak assigned to Q^3 sites is significantly downfield from that of Q^3 (OH) sites in hydrated amorphous silica (−99 to −102 ppm) [35,36], and some samples with Q^3 sites do not have a Q^4 peak (CSHFS6 and SCFUMh). Thus, the Q^3 sites in these samples appear to be part of the C-S-H structure.

The polymerization of our C-S-H samples as expressed by the $Q^1/\Sigma Q^i$ (i = 1–3) ratios decreases with increasing C/S ratio (Figure 5 and Table 4). The straight line in Figure 5 is a fit for all the single-phase samples and has a correlation coefficient of 0.9. However, the samples of the three series have slightly different correlations, and the correlations are not linear. It has been previously observed that the $Q^1/\Sigma Q^i$ ratio of C-S-H does not change significantly for C/S >1.2 [17]. For our C-S-H samples at C/S > ca. 1.3, the polymerization decreases less rapidly than at lower C/S ratios but does continue to decrease. Samples containing portlandite have polymerizations similar to the single-phase samples with the largest C/S ratios.

The ^{29}Si NMR spectra also show some differences that do not obviously correlate with composition. For example, the resolution of the spectra is different for different samples. Some Q^2 peaks have a resolvable downfield (less negative) shoulder located at ca. −82.5 ppm. This shoulder appears in all three series (e.g., SCFUMi, SEWCS1, and CSHFS2), and its resolution is independent of C/S ratio. A downfield shoulder also occurs on some Q^1 peaks, especially for samples in the SEWCS series.

Discussion

Structure of C-S-H

CONTINUITY, DIVERSITY, AND STRUCTURAL CLASSIFICATION. Based on the data in this article, our ^{17}O NMR and

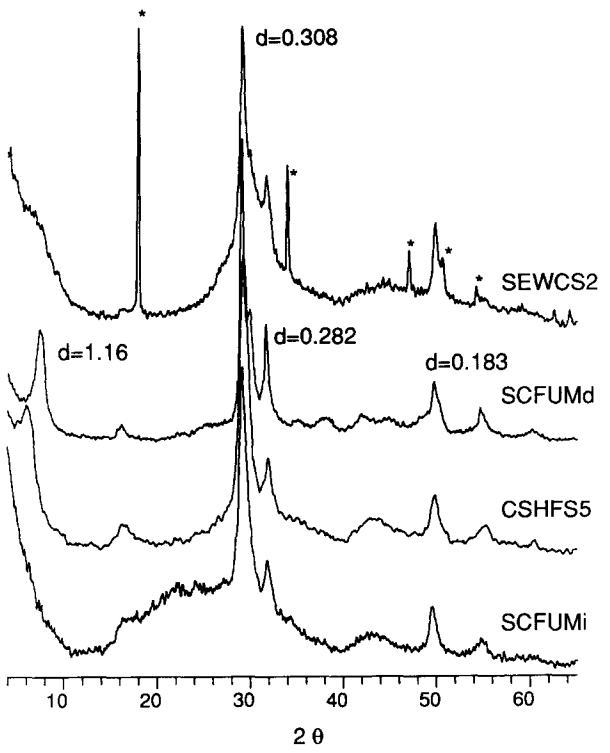

FIGURE 3. X-ray diffraction powder patterns of selected C-S-H samples. Peaks marked with an asterisk are due to portlandite.

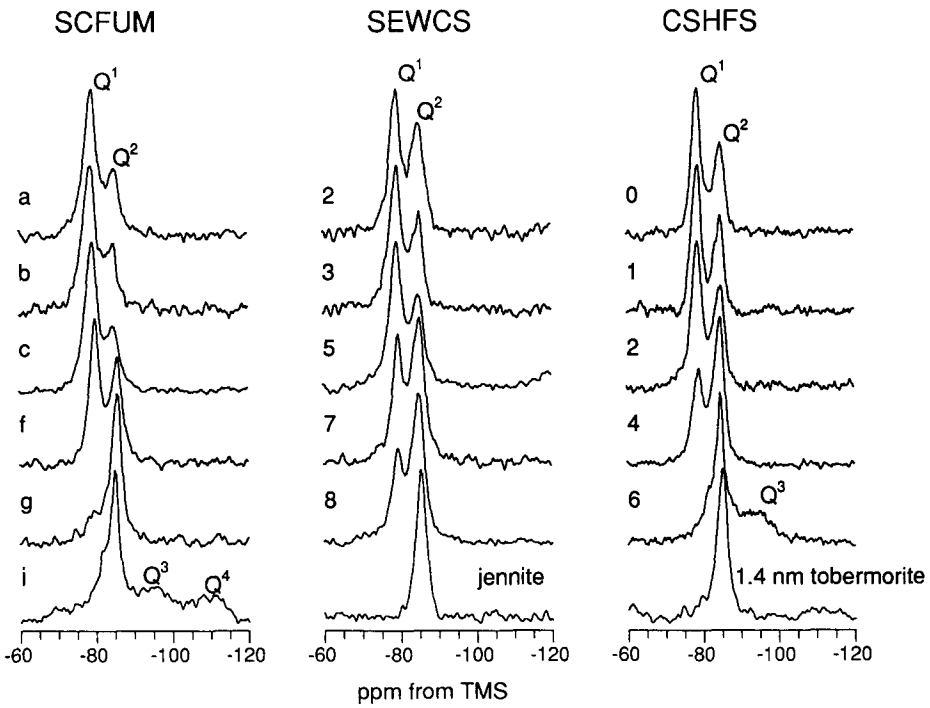

FIGURE 4. Selected ^{29}Si MAS NMR spectra of C-S-H samples of the three sample series. Also shown are ^{29}Si MAS NMR spectra of 1.4-nm tobermorite (C/S = 0.9) and jennite (C/S = 1.4) [26].

^{1}H-^{29}Si cross-polarization magic angle spinning (CPMAS) NMR studies of C-S-H [27,28], and published results [13,15,17], we consider C-S-H in the composition range we observed to be a single phase with a structure that varies continuously with varying composition. There is no structural evidence for multiple C-S-H phases. For single-phase C-S-H, most of the observable characteristics for samples within one synthesis series change systematically with composition, and there are few discontinuous changes. There are continuous changes in the silicate polymerization and pseudo-cell dimensions, solution Ca^{2+} concentrations and pH values, H_2O^+ and H_2O^- contents, and ^{17}O MAS and ^{1}H-^{29}Si CPMAS NMR spectra [27,28].

C-S-H also shows diversity in that samples with similar composition made by different methods may have different silicate polymerizations and cell dimensions. This diversity is not due to the occurrence of fundamentally different kinds of C-S-H, but rather to the effects of, for example, different starting materials, water/solid (w/s) ratios, reaction times, and curing and drying conditions on the same fundamental C-S-H structure. For a C-S-H sample with a known C/S ratio, for instance, it would not be possible to predict the XRD basal reflection, $Q^1/\Sigma Q^i$ ratio, and water content with any accuracy, and vise versa. This diversity is probably the reason why the ^{29}Si NMR spectra of C-S-H samples described in different publications are so different.

Taylor has proposed the existence of two C-S-H phases, C-S-H(I) and C-S-H(II). C-S-H(I) has relatively low C/S ratios (<1.5) and is supposedly structurally related to 1.4-nm tobermorite [12]. C-S-H(II) has relatively higher C/S ratios (>1.5) and is supposedly structurally related to jennite [37]. C-S-H(I) can be formed readily using many methods, but C-S-H(II) is very difficult to form. Based on this classification, all of our C-S-H samples and most described in previous publications would be C-S-H(I). There are only a few reports of successful synthesis of C-S-H(II) in the 1950s [1,38,39] but none in the past 30 years.[2]

We have followed one of the published procedures [38] to produce C-S-H(II) but obtained C-S-H(I). Our data show that samples with bulk C/S ratio > 1.5 are mixtures of C-S-H and portlandite. The importance and even the existence of C-S-H(II) is, thus, unclear. The diversity of our samples is clearly unrelated to C-S-H(II).

Grutzeck et al. have proposed that silica-rich C-S-H (C/S <1) and lime-rich C-S-H (C/S >1) are different phases [15] but did not describe specific structural dif-

[2]Hara et al. [40] considered the intermediate products for jennite synthesis to be C-S-H(II) but gave no details. The intermediate products in our jennite synthesis yield two broad XRD peaks without a basal reflection. The $Q^1/\Sigma Q^i$ ratio of ca. 0.45 for this intermediate product indicates a greater polymerization than for room temperature C-S-H, consistent with the higher synthesis temperature of 80°C.

TABLE 4. ^{29}Si NMR relative peak intensities (%) of the three C-S-H sample series

SEWCS Series							
Sample	**#1**	**#2**	**#3**	**#5**	**#6**	**#7**	**#8**
Q^1	57.5	52.2	61.2	58.3	46.4	42.9	32.4
Q^2	42.5	47.8	38.7	42.0	53.6	57.1	67.6

CSHFS Series							
Sample	**#0**	**#1**	**#2**	**#3**	**#4**	**#5**	**#6**
Q^1	59.0	62.3	55.2	54.7	40.9	20.4	5.2
Q^2	41.0	37.7	44.8	45.3	59.1	79.6	61.5
Q^3							33.3

SCFUM Series									
Sample	**a**	**b**	**c**	**d**	**e**	**f**	**g**	**h**	**i**
Q^1	73.3	69.9	72.8	68.7	65.0	57.2	17.5	9.6	4.5
Q^2	26.7	30.1	27.3	31.3	35.1	42.8	82.6	74.5	49.9
Q^3								16.0	28.6
Q^4									17.0

ferences. Our data show that the structural differences between C-S-H with C/S >1.0 and <1.0 are no greater than the differences among samples with C/S ratios > 1.0 (e.g., Figures 2–5). The only significant difference at low C/S ratios is the occurrence of Q^3 sites in some samples with C/S <0.8. Thus, we find no evidence in our data for the existence of two thermodynamically distinct C-S-H phases.

STRUCTURAL MODELS. There has long been evidence that C-S-H has a layer structure similar to that of tobermorite and/or jennite [13,24], but only the average structure of 1.1-nm tobermorite, $Ca_{2.25}[Si_3O_{7.5}(OH)_{1.5}] \cdot H_2O$, has been solved. This structure contains layers of distorted CaO polyhedra sandwiched between two crystallographically different dreierketten silicate chains [41]. There are additional Ca atoms and H_2O molecules in the interlayer space and significant stacking disorder. Based on powder XRD and NMR data, the structure of 1.4-nm tobermorite, $Ca_5(Si_6O_{18}H_2) \cdot 8H_2O$, is probably similar to that of 1.1-nm tobermorite with more water molecules and Ca^{2+}'s in the interlayers [8,26].

The structure of jennite, $Ca_9(Si_6O_{18}H_2)(OH)_8 \cdot 6H_2O$, is thought to be generally similar to that of tobermorite [8]. The proposed main difference is that about half of the oxygen sites on the CaO polyhedra layers are not linked to silicate chains but to OH^- groups. The silicate chains and rows of OH^- groups parallel to the **b** axis are thought to alternate, resulting in a longer **a** axis than that for tobermorite [8]. ^{29}Si NMR spectra of jennite contain mainly Q^2 sites (Figure 4) [26], consistent with a single-chain structure.

We propose here a defect-tobermorite structural model for C-S-H, in which the structure is based on that of 1.4-nm tobermorite but is more disordered and contains a significant concentration of defects. As in tobermorite, there are Ca^{2+} ions and H_2O molecules in the interlayers. The structure of the layers appears to vary between two cases shown schematically in Figure 6. One kind is an almost perfect tobermorite layer, but

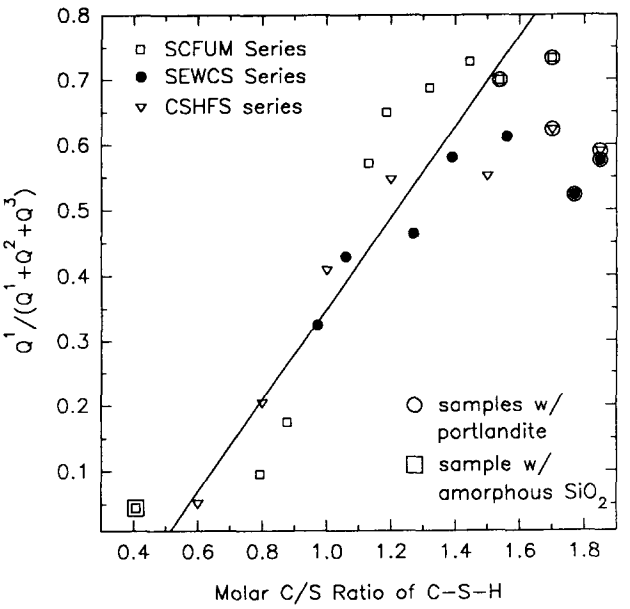

FIGURE 5. Relationship between NMR $Q^1/\Sigma Q^i$ ratio (i = 1, 2, 3) and C/S ratio of all our C-S-H samples, showing the decrease of polymerization as C/S increases. There is an approximately 5% error in the $Q^1/(Q^1 + Q^2 + Q^3)$ ratio due to errors in relative intensities, which are obtained by curve fitting the ^{29}Si MAS NMR spectra. The correlation coefficient for the straight line is 0.9, which is a fit for single-phase samples only, because the C/S ratio of C-S-H in samples containing portlandite is unknown.

with some missing bridging tetrahedra (BT), resulting in depolymerization and disorder. The other kind is highly distorted, contains mostly dimers due to the absence of most BT, and may have fragments of entire chains missing. The tetrahedra are tilted, rotated, and displaced relative to the CaO layers, possibly in ways similar to the disorder mechanisms in 1.1-nm tobermorite [41]. The two types of layers may merge into or occur with each other within a single layer; different types of layers may be stacked together or be present in widely separated parts of the sample. The stacking disorder among adjacent layers and structural disorder within each layer allow for the diversity observed among different C-S-H samples. In cement pastes, $Ca(OH)_2$ layers may also occur within the stacking sequences, further increasing the disorder and C/S ratio.

In his pioneering work on C-S-H, Taylor proposed a structural model in which most C-S-H samples are composed of structurally imperfect jennite layers and only a small portion have a structure similar to that of 1.4-nm tobermorite [13]. The main difference between our model and that of Taylor is that ours focuses on the similarity and importance of tobermorite to C-S-H, whereas his focuses on the importance of jennite. Both jennite and 1.4-nm tobermorite are single-chain hydrated calcium silicates and resemble each other and C-S-H in many aspects, such as composition, ^{29}Si MAS, CPMAS, and ^{17}O NMR spectra. The XRD data indicate that the average structure of our C-S-H is more similar to that of 1.4-nm tobermorite than to jennite. C-S-H and jennite have different pseudo-cell dimensions (Table 3). The **a** axis of jennite is 0.995 nm, significantly larger than that of our C-S-H. On the other hand, the **a** and **b** cell dimensions of 1.4-nm tobermorite are 0.564 and 0.366 nm, respectively, the same as those of our C-S-H, which range from 0.561 to 0.566 nm for **a** and 0.364 to 0.368 for **b**. When the C/S ratio of the C-S-H sample is similar to that of 1.4-nm tobermorite (0.88; e.g., SCFUMg), its XRD pattern, ^{29}Si MAS/CPMAS, and ^{17}O NMR spectra are all more similar to those of 1.4-nm tobermorite than those of C-S-H samples with other C/S ratios. Sample SCFUMg (C/S = 0.88) can be thought of as a poorly crystallized 1.4-nm tobermorite. However, C-S-H samples with C/S ratios similar to jennite (1.4–1.5; e.g., SEWCS4–5, SCFUMc, and CSHFS2) yield ^{29}Si NMR spectra dominated by Q^1 peaks, whereas the spectrum of jennite contains essentially only a Q^2 peak (Figure 4).

Because C-S-H is less polymerized than 1.4-nm tobermorite and jennite, any meaningful structural model for it must provide a structural description of this depolymerization. In our defect-tobermorite structural model, the model compound, 1.4-nm tobermorite, has a C/S ratio of 0.9 and contains long dreieretten (mostly Q^2 sites). The $Q^1/\Sigma Q^i$ ratios of C-S-H samples with C/S <0.9 are less than 0.2, corresponding to relatively long silicate chains comparable to those of disordered 1.4-nm tobermorite. As the C/S ratio increases, the polymerization of the C-S-H decreases, resulting in $Q^1/\Sigma Q^i$ ratios greater than 0.5. This net depolymerization can be achieved in many ways, one is by omission of BT in the dreierketten as first suggested by Taylor [13]. Removal of one BT produces 2 Q^1 Si sites and reduces the chain length. If m represents the fraction of BT that is removed ($0 < m \leq 1$), the resulting C/S ratio is

$$C/S = r \Big/ \left(1 - \frac{m}{3}\right), \tag{1}$$

with r being the initial C/S ratio. The resulting $Q^1/(Q^1 + Q^2)$ ratio ($Q^1/\Sigma Q^i$) is, thus,

$$Q^1/\Sigma Q^i = 2 \Big/ \left(\frac{3}{m} - 1\right). \tag{2}$$

In this model, m increases as the C/S ratio increases, and progressively more BT are omitted, resulting in thinner layers. This idea is consistent with the XRD observation that basal spacings decrease with increasing C/S ratio, although loss of interlayer water may be more important.

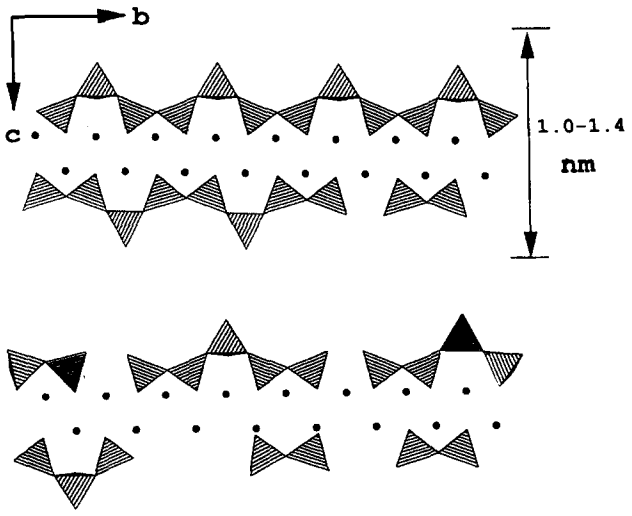

FIGURE 6. Proposed defect-tobermorite structural model for C-S-H, showing dreierketten and central CaO layers (filled circles). The interlayer Ca^{2+}, OH^- groups, and H_2O molecules are omitted. The layer on top represents a relatively perfect 1.4-nm tobermorite layer, in which only a small portion of the bridging tetrahedra is missing, and the chains are relatively long. The layer on the bottom represents a distorted layer, in which individual tetrahedra and an entire chain may tilt, rotate, or be displaced along the **b** axis. Most bridging tetrahedra are missing, resulting in many dimers, and entire segments of silicate chains may also be missing.

Advn Cem Bas Mat
1996;3:144–156

If all the BT are missing (m = 1), a tobermorite-like layer would have a C/S ratio of 1.35, and only Q^1 tetrahedra would be present. Our single-phase C-S-H has C/S ratios up to ca. 1.5 but polymerizations greater than Q^1 sites only, indicating that not all the BT are missing. Thus, at least for C-S-H samples with C/S ratios > 1.35, other defects must occur. These defects could include $Ca(OH)_2$ environments and loss of entire chain segments (both BT and PT). These defects could yield C-S-H with C/S ratios much greater than 1.35. With entire sections of chains missing, the local structure could be similar to that of jennite. Whatever the proportions of these defects, it is clear that C-S-H with C/S ratios similar to that of jennite (ca. 1.5) does not have an average structure similar to jennite. For these C-S-H's, the average structures are still similar to that of 1.4-nm tobermorite as shown by our XRD data, and there is no evidence that they are mixtures of 1.4-nm tobermorite and jennite. This conclusion is consistent with the transmission electron microscopy (TEM) observations of C-S-H structure [42,43].

A jennite-based model cannot accommodate C-S-H with C/S ratios < 1.5 without the addition of silicate chains. Depolymerization of jennite by omission of BT increases the C/S ratio, and it is impossible to make both the structure and composition simultaneously approach those of C-S-H. For example, a $Q^1/\Sigma Q^i$ ratio of 0.5 would yield a C/S ratio of 1.88. For most C-S-H, this $Q^1/\Sigma Q^i$ is unrealistically small and the C/S ratio is too large. Our own data and most published ^{29}Si NMR spectra of C-S-H formed under normal conditions (e.g., [15–18]) indicate that for C/S >1.2, Q^1 Si sites dominate ($Q^1/\Sigma Q^i \geqslant 0.5$). Our single phase C-S-H with the highest C/S ratio (1.56, SEWCS3) has a $Q^1/\Sigma Q^i$ of 0.61. Other samples may have even higher $Q^1/\Sigma Q^i$ ratios (e.g., $Q^1/\Sigma Q^i$ = 0.73 for SCFUMc).

The compositional relationship among C-S-H, 1.4-nm tobermorite, and jennite is illustrated in Figure 7, in which the linear correlations between C/S ratio and $Q^1/\Sigma Q^i$ ratio for 1.4-nm tobermorite and jennite are calculated based on the aforementioned equations; and the straight line for C-S-H is taken from Figure 5. It is clear that the correlation for C-S-H is closer to 1.4-nm tobermorite than to jennite and that C-S-H does not approach the jennite structure for the entire polymerization range. The high polymerization of jennite prevents it from being a good structural model for C-S-H.

The defect-tobermorite structural model of C-S-H is broadly consistent with "solid-solution" models of C-S-H [25,44–46], in which C-S-H is considered to be a solid solution between Ca-silicate hydrate and $Ca(OH)_2$. Our results provide a structural basis for these models, which are frequently used in thermodynamic modeling of C-S-H.

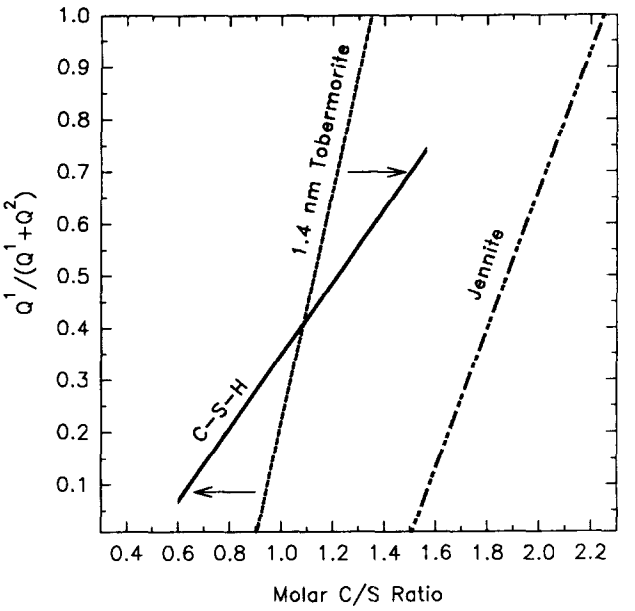

FIGURE 7. Correlation between $Q^1/\Sigma Q^i$ and C/S ratio for C-S-H, 1.4-nm tobermorite, and jennite. Arrows indicate the direction of change of the 1.4-nm tobermorite line as interlayer Ca^{2+} is removed (to the left) and additional Ca-OH sites are added (to the right).

Charge Balance and the Concentration of OH^- Groups

Water molecules (H_2O) and hydroxyl groups (OH^-) are important structural components of C-S-H, but no technique used so far quantitatively and unambiguously distinguishes among water molecules, Ca-OH, and Si-OH groups. Ca-OH bonds have been observed in C-S-H by ^{17}O NMR spectroscopy [19,28], but the existence of Si-OH linkages is still controversial [8]. ^1H-^{29}Si CPMAS NMR demonstrates that ^1H is within a nanometer of Si in C-S-H, because both Q^1 and Q^2 peaks cross-polarize [19,47], but it does not provide conclusive evidence of Si-OH bonds. Si-OH linkage is not required for observation of cross-polarization (CP) signal, as demonstrated by the strong CP signal for Q^4 sites without Si-OH bonds in silica gel [35].

We have carried out charge-balance calculations for C-S-H based on the known C/S and $Q^1/\Sigma Q^i$ ratios and the assumption that the nonbridging oxygens (NBOs) are preferentially balanced by Ca^{2+} [33]. The results demonstrate the presence of both Si-OH and Ca-OH sites in C-S-H (Figure 8). Single-phase C-S-H samples with C/S ratios < 1.3 fall on the left of the 1:1 line in Figure 8, indicating that they contain less Ca^{2+} than required for overall charge neutrality. The only other positive species is H^+, thus there must be Si-OH linkages in these samples to balance the charge. Samples with C/S ratio > 1.3 fall on the right of the 1:1 line in Figure 8, indicating that they contain more Ca^{2+}'s than

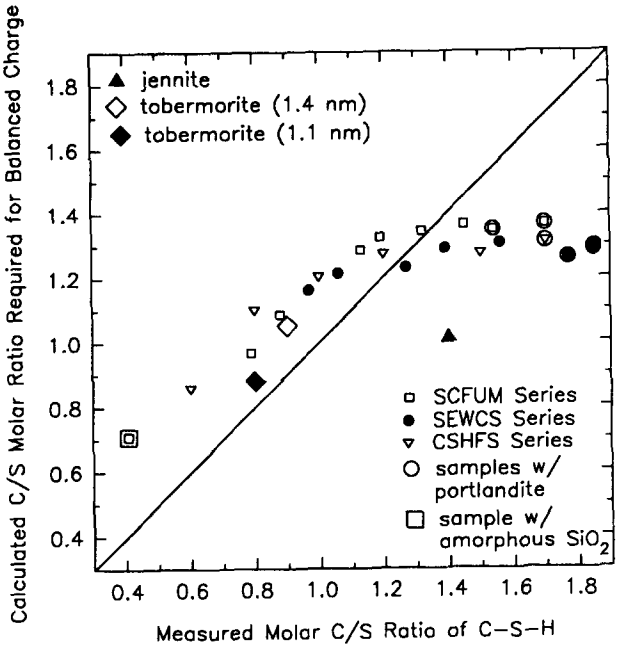

FIGURE 8. Charge-balance calculation for C-S-H. The y-axis is the calculated, minimum C/S ratio needed for balanced charge. The straight line represents an 1:1 ratio of the calculated and measured C/S ratios. Points on the left of the straight line represent samples that are Ca^{2+} deficient for charge balance. Points on the right of the straight line represent samples that have excess Ca^{2+}. Also shown are data for tobermorite (both 1.1- and 1.4 nm varieties) and jennite.

needed to neutralize the NBOs. These excess Ca^{2+}'s must form Ca-OH bonds. Ca-OH bonds could also be present at lower C/S ratios for which there is not enough Ca^{2+} for charge balance, and their presence would require an equal number of additional Si-OH bonds to maintain overall charge neutrality. Similarly, Si-OH bonds could also occur at C/S ratios greater than 1.3 if there are additional Ca-OH bonds. This idea is consistent with ^{17}O NMR results [28]. At larger C/S ratios, structural regions with high concentrations of Ca-OH bonds may be detectable by XRD as portlandite.

The critical C/S ratio of approximately 1.3 in these charge-balance calculations is due to the limitation of the 1.4-nm tobermorite structure and supports the idea that the increase of C/S ratio and depolymerization of C-S-H are due to absence of BT in the dreierketten. As discussed earlier, the largest C/S ratio obtained by omission of all BT (m = 1) in tobermorite is 1.35, whereas the calculated C/S ratio of 1.3 required for charge balance for C-S-H is independent of the structural model.

The charge-balance calculations also demonstrate that the C-S-H structure is quite dissimilar to that of jennite. 1.4-nm tobermorite falls on the same trend as C-S-H in Figure 8, whereas jennite falls far from it.

The minimum mole percent of both Si-OH and Ca-OH can be readily calculated from the vertical distance of a point to the straight line in Figure 8. The results (Figure 9) show that the minimum mole percent of Si-OH bonds decreases from ca. 12% to 0 as the C/S ratio varies from 0.80 to 1.35 and that the minimum mole percent of Ca-OH increases from ca. 0 to 19% as the C/S ratio increases from 1.35 to 1.85.

Limits on the abundance of Si-OH and Ca-OH bonds in C-S-H can also be calculated from a different approach based on the known $Q^1/\Sigma Q^i$ and C/S ratios and the defect-tobermorite structural model. ^{1}H-^{29}Si CPMAS NMR data of our C-S-H show that both Q^1 and Q^2 sites have similar amounts of Si-OH bonds regardless of whether they occur in short dreierkettens or dimers [27]. Our unpublished infrared (IR) data indicate that the concentration of Si-OH bonds in C-S-H decreases with increasing C/S ratio, whereas Ca-OH bonds seem to be present for all samples. Based on these observations, it can be shown that only 0–33% of NBOs on both Q^1 and Q^2 sites in C-S-H can form Si-OH bonds [33], and the percentage decreases with increasing C/S ratio. Assuming that the percentage of NBOs forming Si-OH bonds varies linearly from 33% for C/S = 0.88 (the smallest C/S ratio of single-phase C-S-H without Q^3 Si sites) to 0 for C/S = 1.56 (the greatest C/S ratio of single-phase C-S-H), the concentrations of Si-OH and Ca-OH bonds for C-S-H of various compositions can be calculated by neutralizing the NBOs in the order of Si-OH, Si-O-Ca, and Ca-OH.

The results of the calculations indicate that the maximum percentage of NBOs forming Si-OH bonds is much less than 33%, because the resultant total amount of OH^- groups (Ca-OH + Si-OH) is greater than the amount of measured H_2O^+, which is the maximum possible total amount of OH^- groups. Similarly, the maximum percentage must be greater than 16%, because this value yields a total OH^- abundance less than the minimum Si-OH bonds obtained by the charge-balance calculation. For the same reason, the minimum percentage of NBOs forming Si-OH bonds must be greater than 0. Satisfactory results can be obtained when the percentage of NBOs forming Si-OH bonds are allowed to vary between 5% (for C/S = 1.56) and 20% (for C/S = 0.88) (Figure 9).

The calculated concentration of Si-OH linkages corresponding to the curve in Figure 9 is greater than that of Ca-OH for C/S <1.2 and decreases with increasing C/S ratio, whereas that of Ca-OH is very low (<3 mol%) for C/S <1.2 and increases with increasing C/S ratio (Figure 10). In this model, the number of Si-OH bonds per tetrahedron (Si-OH/Si) varies from 0.13 for C/S = 1.56 to 0.43 for C/S = 0.88, with an average of 0.31, which is consistent with the estimated value of 0.33 made by Taylor [48]. The low concentration of Ca-OH

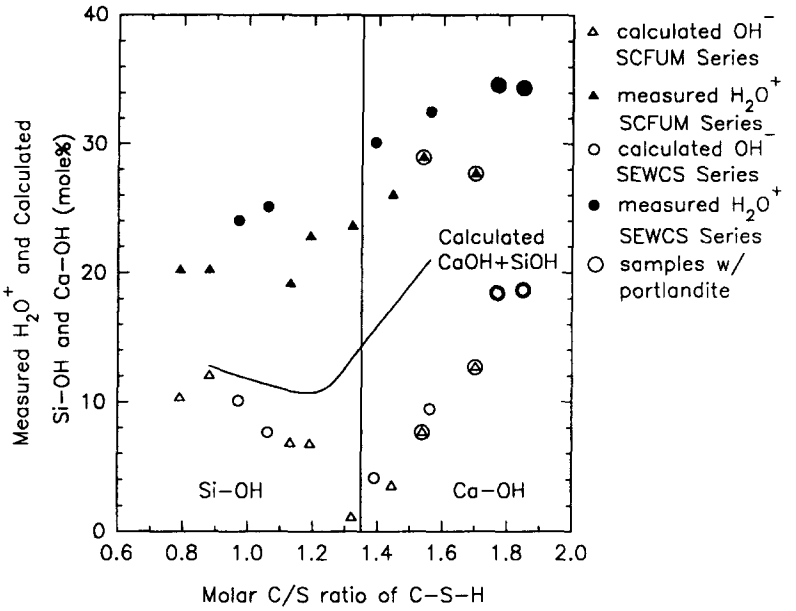

FIGURE 9. Plot of molar C/S ratio of C-S-H against measured H_2O^+ (filled points) and concentrations (open points) of Si-OH (left) and Ca-OH (right) obtained from charge-balance calculations. The vertical line represents the C/S ratio at which the overall electrical charge is balanced. The curve represents the minimum concentrations of OH^- groups (Si-OH + Ca-OH) obtained by model calculations using 5–20% nonbridging oxygens (NBOs) to form Si-OH bonds. The concentrations of Si-OH and Ca-OH of the model calculations are shown in Figure 10. See text.

bonds (0.2% on average) for C/S <1.2 is consistent with the charge-balance calculation (Figure 8), which shows that there is not enough Ca^{2+} to charge balance all the NBO's. The exact values of the Si-OH and Ca-OH abundances depend critically on the assumed linear variation of the percentage of NBOs forming Si-OH bonds, but the trends and approximate values are clear. Therefore, for single-phase C-S-H with the observed maximum C/S ratio of 1.5 and possible dreierketten, an ideal formula might be $Ca_{4.5}[Si_3O_8(OH)](OH)_4 \cdot nH_2O$.

Silicate Polymerization and C-S-H Composition

One of the most important observations of this study is that the C-S-H samples in all three series with C/S ratio > ca. 1.54 contain portlandite detectable by XRD. Their polymerizations are, thus, greater than their bulk C/S ratios suggest (Figure 5). Therefore, it seems that at least for our samples, single-phase C-S-H has a limiting C/S ratio of ca. 1.5 and a corresponding $Q^1/\Sigma Q^i$ of ca. 0.7. This limiting C/S ratio is significantly less than the widely accepted value of 1.7 for C-S-H in OPC paste [8], possibly due to difficulty in analysis of phase-pure C-S-H in cement paste. Recently, $Ca(OH)_2$ has been found coexisting with C-S-H with a C/S ratio as small as 1.3 [47], supporting this conclusion. It is also possible that the chemical conditions in OPC paste differ significantly enough from those in our experiments that C-S-H with C/S ratios as large as 1.7 could become stable. Such differences may include the existence of alkalis and sulfate phases and substitution of Al or Fe into C-S-H.

The average chain length for most C-S-H samples with low polymerizations determined by NMR does not fully describe the real structure. For instance, the average chain length for SCFUMc (C/S = 1.45, $Q^1/\Sigma Q^i$ = 0.7) is 2.7, shorter than a trimer. However, ^1H-^{29}Si CPMAS data indicate that many dimers and some relatively long chains coexist in the structure [27]. The CPMAS data also indicate that the chains have a bimodal length distribution for samples with C/S >0.9, consistent with the defect-tobermorite structural model.

C-S-H samples with C/S ratios < ca. 0.85 contain Q^3 Si sites, and similar sites have been reported previously [47]. The presence of these sites does not lead to significantly different XRD parameters. Therefore, it is clear that Q^3 sites do occur in single-phase C-S-H with C/S ratios between 0.8 and 0.6. The chemical shifts of the Q^3 sites are similar to those of the Q^3 sites of tobermorite [22,26]. The relationship between Q^3-containing C-S-H and normal C-S-H may be similar to that between normal and anomalous tobermorite. The Q^3 sites in C-S-H can form due to stacking disorder resulting from a **b**/2 displacement of the chains. C-S-H of this type does not occur in OPC paste but may be important in dispersed

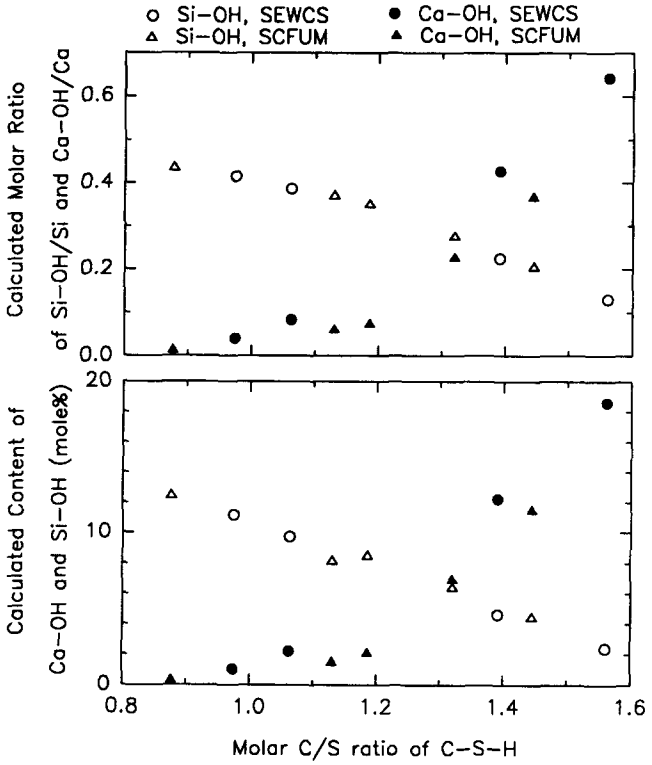

FIGURE 10. Calculated minimum concentrations of Si-OH and Ca-OH bonds (bottom plot) and Si-OH/Si and Ca-OH/Ca ratios (top plot) for phase-pure C-S-H without Q^3 Si sites in the SCFUM and SEWCS series.

small particle (DSP) cement and other cements containing pozzolanic components.

Multiple Q^1 and Q^2 sites in C-S-H

The ^{29}Si MAS NMR peaks of our C-S-H samples are about 4.5 ppm broad at half height, indicating a range of different local structural environments. The peaks for the Q^1 sites are asymmetric or have a small shoulder near approximately −78 ppm in addition to the main peak at −79 ppm (Figure 4). Similarly, the peaks for Q^2 sites are asymmetric or have a small shoulder at ca. −82.5 ppm in addition to the main peak at about −85.5 ppm. The downfield shoulder on the Q^2 peak has also been previously reported [17,36,47,49] with contradictory assignments. A similar downfield shoulder occurs on the Q^2 peak of 1.1-nm tobermorite [20,50,51], but its assignment is also unclear.

It is reasonable to consider that Q^1 sites in dimers and on chain ends might have different local structures and thus yield slightly different chemical shifts, but the assignment is not conclusive.

Multiple Q^2 sites are more difficult to explain. The main peak at ca. −85.5 ppm can be readily assigned to the middle tetrahedra of dreierketten. Many crystalline phases with similar compositions yield NMR peaks with this chemical shift, including 1.1-nm tobermorite [20,22]. The exact chemical shift for the downfield shoulder is hard to determine due to poor resolution, but it appears to be between −82.5 and −84 ppm. The only crystalline calcium silicate with a similar chemical shift known to us is pseudowollastonite, which has a ring structure and a chemical shift of −83.5 ppm [34]. Although there has been report of silicate rings in C-S-H [52], XRD data indicate the opposite; the consensus is that silicate rings are not important in C-S-H [53].

The downfield shoulder is probably due to distorted Q^2 sites produced by various kinds of stacking disorder. Sherriff et al. [54] have found that the ^{29}Si MAS NMR chemical shifts of silicates can be correlated to the local geometry of the structure by a relatively simple model, which can be thought of as the magnetic anisotropy modified by the valence of the bonds between the nearest neighbor (NN) oxygens and the next nearest neighbor (NNN) cations. Although the magnetic anisotropy is a complex parameter, the most important controlling factor is the orientation of the O-M bond (M represents NNN cations) relative to the Si-O bond inside the tetrahedron. Relative to the ordinary Q^2 sites, the downfield shoulder corresponds to a smaller modified magnetic anisotropy, which can be due to decreased Si–O–M bond angles and Si–M distances. The disorder mechanisms discussed in our structural model of C-S-H, such as displacement and tilt of tetrahedra and stacking disorder, may produce such sites.

Recently, Brough et al. [55] have found resolved peaks at about −84 and −86 ppm in a ^{29}Si MAS NMR study of the hydration of mixtures of C_3S and ^{29}Si-enriched amorphous silica and assigned the −84 ppm peak to BT and the −86 ppm peak to PT in dreierketten. This assignment is, however, inconsistent with our observation that for 1.1-nm tobermorite the downfield shoulder is present even when all the BT are cross-linked into Q^3 sites [26].

Thus, assignment of these peaks is an unusually difficult problem that remains unresolved. Quantum chemical calculations to better understand the local Si-environments and the controls of ^{29}Si NMR chemical shifts are needed.

Acknowledgments

This project was done under the auspices of the Center for Advanced Cement Based Materials sponsored by the National Science Foundation and was supported by the grant DOE SBC NU YOUNG ANT. The authors would like to thank Prof. J.F. Young for very helpful discussions.

References

1. Taylor, H.F.W. *J. Chem. Soc.* **1950,** 3682–3690.
2. Kantro, D.L.; Brunauer, S.; Weise, C.H. *Adv. Chem. Ser.* **1961,** *33,* 199–219.

3. Grutzeck, M.W.; Roy, D.M. *Nature* **1969,** *223,* 492–494.
4. Groves, G.W.: Sueur, P.J.L.; Sinclair, W. *J. Am. Ceram. Soc.* **1986,** *69,* 353–356.
5. Locher, F.W. In *Symposium on Structure of Portland Cement Paste and Concrete* (Sp. Rpt. 90). Highway Research Board: Washington, DC, 1966; pp 300–308.
6. Taylor, H.F.W.; Turner, A.B. *Cem. Concr. Res.* **1987,** *17,* 613–623.
7. Mindess, S.; Young, J.F. *Concrete.* Prentice-Hall: Englewood Cliffs, NJ, 1981.
8. Taylor, H.F.W. *Cement Chemistry.* Academic Press; London, 1990.
9. Young, J.F.; Hansen, W. *Mater. Res. Soc. Symp. Pro.* **1987,** *85,* 313–322.
10. Brunauer, S.; Kantro, D.L.; Copeland, L.E. *J. Am. Chem. Soc.* **1958,** *80,* 761–767.
11. Taylor, H.F.W. *J. Chem. Soc.* **1953,** 163–171.
12. Taylor, H.F.W. *Proc. 5th. Int. Symp. Chem. Cem.* **1968,** *2,* 1–26.
13. Taylor, H.F.W. *J. Am. Ceram. Soc.* **1986,** *69,* 464–467.
14. Jennings, H.M. *J. Am. Ceram. Soc.* **1986,** *69,* 614–618.
15. Grutzeck, M.; Benesi, A.; Fanning, B. *J. Am. Ceram. Soc.* **1989,** *72,* 665–668.
16. Lippmaa, E.; Mägi, M.; Tarmak, M.; Wieker, W.; Grimmer, A.R. *Cem. Concr. Res.* **1982,** *12,* 597–602.
17. Macphee, D.E.; Lachowski, E.E.; Glasser, F.P. *Adv. Cem. Res.* **1988,** *1,* 131–137.
18. Young, J.F. *J. Am. Ceram. Soc.* **1988,** *71,* C-118–C-120.
19. Cong, X.; Kirkpatrick, R.J. *Cem. Concr. Res.* **1993,** *23,* 1065–1077.
20. Wieker, W.; Grimmer, A.R.; Winkler, A.; Mägi, M.; Tarmak, M.; Lippmaa, E. *Cem. Concr. Res.* **1982,** *12,* 333–339.
21. Rodger, S.A.; Groves, G.W.; Clayden, N.J.; Dobson, C.M. *J. Am. Ceram. Soc.* **1988,** *71,* 91–96.
22. Bell, G.M.M.; Bensted, J.; Glasser, F.P.; Lachowski, E.E.; Roberts, D.R.; Taylor, M.J. *Adv. Cem. Res.* **1990,** *3,* 23–37.
23. Heller, L.; Taylor, H.F.W. *Crystallographic Data for the Calcium Silicates.* Her Majesty's Stationery Office: London, 1956.
24. Taylor, H.F.W. *Zeit. Kristall.* **1992,** *202,* 41–50.
25. Richardson, I.G.; Groves, G.W. *Cem. Concr. Res.* **1992,** *22,* 1001–1010.
26. Cong, Z.; Kirkpatrick, R.J. *Adv. Cem. Based Mater.* **1996,** *3,* 133–143.
27. Cong, X.; Kirkpatrick, R.J. *Adv. Cem. Res.* **1995,** *7,* 103–112.
28. Cong, X.; Kirkpatrick, R.J. *J. Am. Ceram. Soc.,* in press.
29. Cong, X.; Kirkpatrick, R.J. *Cem. Conc. Res.* **1995,** *25,* 1237–1245.
30. Nettleship, I.; Shull, J.L., Jr.; Kriven, W.M. *J. Euro. Ceram. Soc.* **1993,** *11,* 291–298.
31. Steinour, H.H. *Chem. Rev.* **1947,** *40,* 391–460.
32. Farmer, V.C.; Jeevaratnam, J.; Speakman, K.; Taylor, H.F.W. In *Symposium on Structure of Portland Cement Paste and Concrete* (Sp. Rpt. 90). Highway Research Board: Washington, DC, 1966; pp 291–298.
33. Cong, X. *^{29}Si and ^{17}O Nuclear Magnetic Resonance Investigation of the Structure of Calcium Silicate Hydrate Phases,* PhD Thesis. University of Illinois at Urbana-Champaign, 1994.
34. Mägi, M.; Lippmaa, E.; Samoson, A.; Engelhardt, G.; Grimmer, A.R. *J. Phys. Chem.* **1984,** *88,* 1518–1522.
35. Maciel, G.F.; Sindorf, D.W. *J. Am. Chem. Soc.* **1980,** *102,* 7606–7607.
36. Cong, X.; Kirkpatrick, R.J. *Cem. Concr. Res.* **1993,** *23,* 811–823.
37. Gard, J.A.; Taylor, H.F.W. *Cem. Concr. Res.* **1976,** *6,* 667–678.
38. Brunauer, S.; Greenberg, S.A. *Proc. 4th Int. Sym. Chem. Cem.* **1960,** *1,* 135–165.
39. Copeland, L.E.; Schulz, E.G. *J. PCA Res. Dev. Labs.* **1962,** *4,* 2–12.
40. Hara, N.; Inous, N. *Cem. Concr. Res.* **1980,** *10,* 677–682.
41. Hamid, S.A. *Zeit. Kristall.* **1981,** *154,* 189–198.
42. Henderson, E.; Bailey, J.E. *J. Mater Sci.* **1988,** *23,* 501–508.
43. Melzer, R.; Eberhard, E. *Cem. Concr. Res.* **1989,** *19,* 411–422.
44. Kantro, D.L.; Brunauer, S.; Weise, C.H. *J. Phys. Chem.* **1962,** *66,* 1804–1809.
45. Stade, H.; Wieker, W. *Z. Anorg. Allg. Chem.* **1980,** *466,* 55–77.
46. Glasser, F.P.; Lachowschi, E.E.; Macphee, D.E. *J. Am. Ceram. Soc.* **1987,** *70,* 481–485.
47. Okada, Y.; Ishida, H.; Mitsuda, T. *J. Am. Ceram. Soc.* **1994,** *77,* 765–768.
48. Taylor, H.F.W. *Adv. Cem. Based Mater.* **1993,** *1,* 38–46.
49. Groves, G.W.; Rodger, S.A. *Adv. Cem. Res.* **1989,** *2,* 135–140.
50. Sato, H.; Grutzeck, M. *Mater. Res. Soc. Proc.* **1992,** *245,* 235–240.
51. Mitsuda, T.; Toraya, H.; Okada, Y.; Shimoda, M. *Ceram. Trans.* **1988,** *5,* 206–213.
52. Lentz, C.W. In *Symposium on Structure of Portland Cement Paste and Concrete* (Sp. Rpt. 90). Highway Research Board: Washington, DC, 1966; 269–283.
53. Bailey, J.E.; Stewart, H.R. *Proc. Br. Ceram. Soc.* **1984,** *35,* 193–206.
54. Sherriff, B.L.; Grundy, H.D. *Nature* **1988,** *332,* 819–822.
55. Brough, A.R.; Dobson, C.M.; Richardson, I.G.; Groves, G.W. *J. Am. Ceram. Soc.* **1994,** *77,* 593–596.
56. Gard, J.A.; Taylor, H.F.W.; Cliff, G.; Lorimer, G.W. *Am. Mineral.* **1977,** *62,* 365–368.